Template-Directed Assembly of Metal–Chalcogenide Nanocrystals into Ordered Mesoporous Networks

Ioannis Vamvasakis,[†] Kota S. Subrahmanyam,[‡] Mercouri G. Kanatzidis,[‡,§] and Gerasimos S. Armatas*[,†]

[†]Department of Materials Science and Technology, University of Crete, Vassilika Vouton, Heraklion 71003, Crete, Greece, [‡]Department of Chemistry, Northwester University, 2145 Sheridan Road, Evanston, Illinois 60208, United States, and [§]Materials Science Division, Argonne National Laboratory, Argonne, Illinois 60439, United States

ABSTRACT Although great progress in the synthesis of porous networks of metal and metal oxide nanoparticles with highly accessible pore surface and ordered mesoscale pores has been achieved, synthesis of assembled 3D mesostructures of metal–chalcogenide nanocrystals is still challenging. In this work we demonstrate that ordered mesoporous networks, which comprise well-defined interconnected metal sulfide nanocrystals, can be prepared through a polymer-templated oxidative polymerization process. The resulting self-assembled mesostructures that were obtained after solvent extraction of the polymer template impart the unique combination of light-emitting metal chalcogenide nanocrystals, three-dimensional open-pore structure, high surface area, and uniform pores. We show that the pore surface of these materials is active and accessible to incoming molecules, exhibiting high photocatalytic activity and stability, for instance, in oxidation of 1-phenylethanol into acetophenone. We demonstrate through appropriate selection of the synthetic components that this method is general to prepare ordered mesoporous materials from metal chalcogenide nanocrystals with various sizes and compositions.

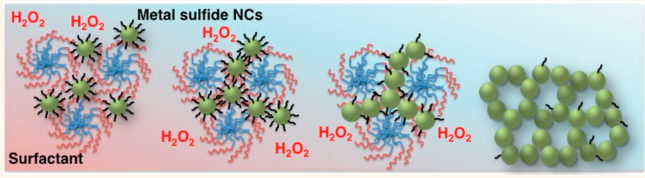

KEYWORDS: mesoporous semiconductors · metal chalcogenides · self-assembly · nanoparticles

Synthesis of mesoporous (pore size from 2 to 50 nm) assembly architectures from inorganic nanocrystals (NCs) represents an important challenge in material science and chemical nanotechnology. Such self-assembled materials can incorporate complementary functionalities such as nanoporosity and quantum-confined electronic properties of individual NCs into the same structure, which endow them with potential applications in photocatalysis, solar energy conversion, chemical sensing and size-selective adsorption and separation.[1−3] Beyond the distinctive optical, electronic and catalytic properties inherent to the nanocrystal building blocks, three-dimensional (3D) networks of inorganic NCs, however, are expected to benefit from the large accessible pore surface and facile diffusion of the target molecules. Furthermore, self-assembled formulations of nanoparticles may exhibit new collective properties due to the interaction of properties of the primary constituents.[4]

During the last years, significant research efforts have been devoted on using structure-directing molds of organic polymers to assemble mesoscopic architectures from colloidal NCs. In general, this method involves favored enthalpic interactions of inorganic nanobuilding blocks with preassembled block copolymer scaffolds, which provide precise control at the mesoscale range.[5] However, even though amphiphilic templating has been shown to produce ordered mesoporous metal (*e.g.*, Pt)[6] and metal oxide (*e.g.*, Mn_3O_4, Fe_2O_3, TiO_2, CeO_2) NC-based networks,[7,8] a simple extrapolation of this approach to mesoporous chalcogenide materials is very difficult. The problem is that, unlike to mesoporous oxides, thermal processing cannot be considered as a reproducible way to remove the polymer template and fuse the metal chalcogenide NCs into an extended three-dimensional structure. Moreover, the porous structure needs to survive destruction of the assembled framework during template removal process. Previous efforts for assembling porous networks from metal–chalcogenide NCs (*e.g.*, CdS(Se), ZnS, PbS)

* Address correspondence to garmatas@materials.uoc.gr.

Received for review February 12, 2015 and accepted April 10, 2015.

Published online April 14, 2015
10.1021/acsnano.5b01014

employ template-free synthetic routes, which have resulted in nanocrystal-based aerogels.[9] These inorganic polymers, although possessing large and accessible pore volume, they exhibit poor ordering with limited control over pore size and surface area. Recently, polymer-templating of ligand-stripped CdSe NCs for assembling porous thin-film semiconductors has been reported.[10] While this method may produce NC-based conductive films, only thermally stable metal chalcogenide NCs can be assembled as they must fuse into a continuous network at a temperature below the degradation point of the polymer template.

Here we propose, for a first time, a synthetic strategy that allows us to assemble metal chalcogenide NCs into ordered 3D mesoporous networks with high internal surface area and uniform pores. We have chosen to explore the assembly of CdS mesostructures because of their ensuing optical, electronic and photocatalytic properties, and the facile production of starting nanoparticles.[11,12] Thus, by taking advantage of the recent synthetic techniques for elaborating ligand-stabilized NCs, we produced water-soluble CdS NCs with different size (*i.e.*, from ~4 to ~6.5 nm) and we used them as starting building blocks to assemble ordered mesoporous structures with the aid of surfactants. More importantly, this method has allowed us to construct ordered mesoporous architectures with different size and composition of the metal sulfide nanobuilding blocks. These unique porous materials demonstrate optical absorption properties consistent with quantum confinement, which are derived from the constituting NCs of the assembled structure. We show that the pore surface of these chalcogenide networks is highly active and accessible to incoming molecules, exhibiting high photocatalytic activity and stability, for instance, in aerobic oxidation of 1-phenylethanol into acetophenone.

RESULTS AND DISCUSSION

The synthesis of mesoporous CdS NC assemblies is accomplished in a single-step chemical process in which the organization and self-polymerization of colloidal NCs into 3D polymeric networks are simultaneously achieved. In particular, we utilized commercially available polyoxoethylene-*block*-cetyl ether (designated as POE(20)-*b*-C16 or Brij 58) block copolymer to template the organized cross-linking polymerization of ligand-stabilized CdS NCs. Among various capping agents for CdS NCs, we selected 3-mercaptopropionic acid (3-MPA). The 3-MPA ligand bears a thiolate group able to bind to the NC's surface and an end-point propionic acid functional group, which is anticipated to engage in enthalpic interactions with the polar POE block of the polymer template. Such interactions can favor the formation of mesostructured NC/polymer composites. For the slow depletion of the thiolate ligands from the nanoparticle surface and oxidative polymerization of CdS NCs, we made a small addition of 1 wt % H_2O_2 to the NC−block copolymer solution. The mild oxidation of NC's surface is key to cross-link the colloidal metal sulfide nanoparticles into 3D superstructures by formation of disulfide (or polysulfide) bonds.[13,14] In comparison, when a higher concentration of hydrogen peroxide (5 wt % in water) is being used for the gelation process, the CdS NCs aggregate in an uncontrolled manner yielding nonporous, bulky, hydrogels. Finally, the organic template was carefully removed from the hybrid nanocomposites by a postpreparative treatment in ethanol and water to produce ordered mesoporous structures of CdS NC assemblies (NCA-CdS). We found that a three cycles of ethanol/water washing process is sufficient to eluate most of the organic molecules. Characterization of the mesoporous products by thermogravimetric analysis (TGA) indicates a ~7−8 wt % of organic residue remaining in the pores (Supporting Information Figure S1). Attempts to remove the organic molecules further proved challenging and resulted in degradation of the pore structure as inferred by TGA and N_2 physisorption measurements (see Supporting Information Figures S2 and S3). Moreover, although thermal annealing of samples (under N_2 atmosphere) eliminates completely the organic molecules, it leads to destruction of the nanocrystal network with consequent loss of porosity. However, as we will show later, the remaining organic matter does not impose significant pore restrictions or affect surface properties of the porous structure. Scheme 1 illustrates the overall synthetic procedure of the NCA-CdS mesostructures.

Small-angle X-ray scattering (SAXS) measurements on the mesoporous materials NCA-CdS-4 and NCA-CdS-6 prepared from CdS NCs with different diameter were carried out to verify the mesoscopic ordering. The SAXS patterns, in Figure 1a, display a primary diffraction peak at scattering wave vector q ($=4\pi\cdot\sin\theta/\lambda$, where 2θ is the scattering angle) region of 0.44 and 0.32 nm^{-1} for NCA-CdS-4 and NCA-CdS-6, which corresponds to a d-spacing ($d = 2\pi/q$) of about 14.3 and 19.6 nm, respectively. The presence of these peaks clearly indicates that the as-prepared assembled structures are ordered (or at least have a low degree of polydispersity) at the mesoscale length. To elucidate the structural ordering of templated assemblies, we prepared porous aggregates of 4 and 6.5 nm-sized CdS NCs following a similar procedure described above but in absence of surfactant. In this case, the ligand-to-ligand dispersion forces play a dominant role and guide the nanoparticles into close-packed superlattice assemblies.[15,16] As expected, these materials do not exhibit any distinguishable SAXS scattering peak, which can be considered to be random aggregates of individual CdS NCs (RNA-CdS-4 and RNA-CdS-6, see Supporting Information Figure S4). Analysis of the X-ray scattering data with Guinier approximation

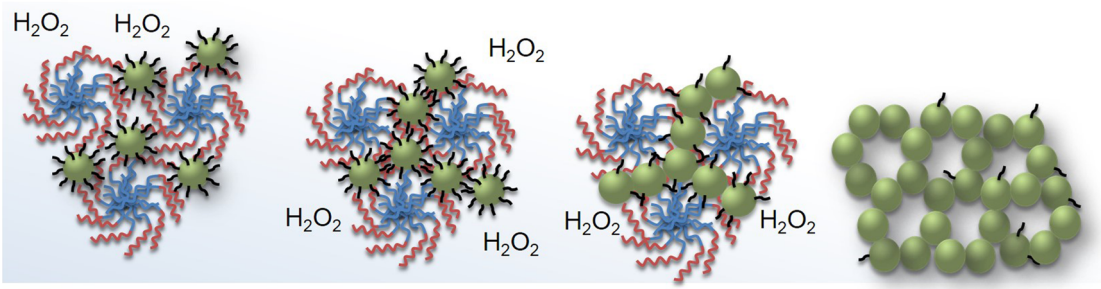

Scheme 1. Schematic illustration showing possible reaction route for the formation of mesoporous CdS NC assemblies (NCA-CdS family).

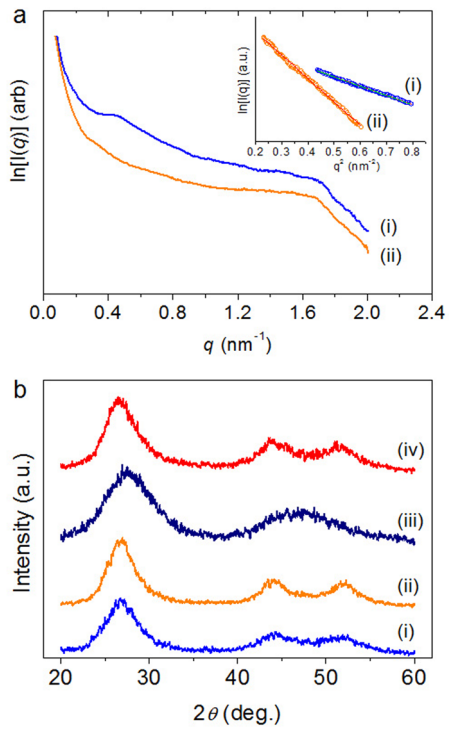

Figure 1. (a) Small-angle X-ray scattering patterns (Inset: the corresponding Guinier plots derived from scattering data. The red lines are fit to the data) and (b) wide-angle X-ray diffraction of mesoporous NCA-CdS-4 (i) and NCA-CdS-6 (ii) materials. The XRD profiles of individual 4 nm (iii) and 6.5 nm (iv) size CdS nanosized building blocks are also given in panel b.

showed that the average grain size of starting CdS nanoparticles did not change with synthesis procedure. The average particle size of the constituent CdS NCs was estimated to be ~3.9 nm for NCA-CdS-4 and ~6.5 nm for NCA-CdS-6 (Figure 1a, inset), which is approximately commensurate with the average particle size of the respective colloidal NCs, *i.e.* ~3.8 and ~6.3 nm, respectively (Supporting Information Figure S5).

Powder X-ray diffraction (XRD) was employed to probe the crystallinity of porous networks. As can be seen in Figure 1b, the XRD patterns of the primary CdS NCs and mesoporous structures are identical, indicating that the cubic crystalline phase of CdS building blocks is persist through the assembly process. In XRD patterns, the mesoporous materials exhibit a remarkably peak broadening of the Bragg reflections corresponding to a very small crystal size. A peak-width analysis using the Scherrer's equation [The average crystallite size (Ds) in all three directions was obtained by $Ds = 0.9 \cdot \lambda/(B \cdot \cos\theta)$, where λ is the wavelength of X-rays (λ_{cu} =1.5418 Å) and B is the full-width at half-maximum of the XRD peak centered at 2θ degrees][17] gives an average domain size of CdS crystallites of about 2.6 nm for NCA-CdS-4 and 3.2 nm for NCA-CdS-6, which is close to that of respective starting materials (~2.1 and ~2.5 nm, respectively). These results, along with the SAXS analysis for CdS particle size, consist that CdS NCs are poly crystal domains.

Figure 2a shows a low-magnification TEM image of the mesoporous NCA-CdS-4. The image depicts uniform mesopores that are locally disordered throughout the assembled structure. A high-magnification image of NCA-CdS-4 mesoporous is shown in Figure 2b, where the presence of individual NCs that fully fuse to form dense wall is visible. Careful analysis of the mesoporous structure gives an average pore diameter of ~6 nm with an average pore wall thickness of about 7–8 nm. The high resolution TEM (HRTEM) demonstrates that CdS NCs have a well crystalline structure, showing lattice fringes throughout the nanoparticles that correspond to (101) planes of cubic CdS (Figure 2b, inset). The crystallinity noted in the XRD patterns was also verified by electron diffraction, which shows broad Debye–Scherrer diffraction rings indexed to the cubic phase of CdS (Figure 2c).

Nitrogen physisorption measurements indicated that our assembled structures possess high porosity with regular mesopores between the connected nanoparticles. In Figure 3, the N_2 adsorption–desorption isotherms represent typical type-IV curves with an H_2-type hysteresis loop according to IUPAC classification, which are characteristic of mesoporous solids with cylindrical pore channels.[18] The small but resolved adsorption step at midrelative pressure region (0.4–0.5 P/P_o) is related to the capillary condensation of nitrogen in narrow sized mesopores.[19] The Brunauer–Emmett–Teller (BET) surface area of NCA-CdS-4 is

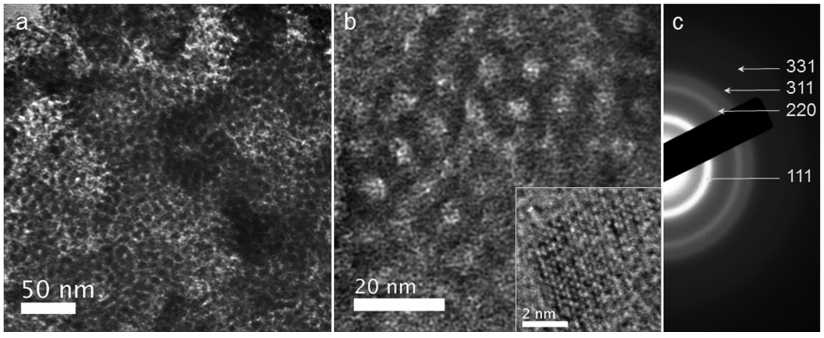

Figure 2. (a and b) TEM images, high-resolution TEM from an individual CdS NC (inset of panel b) demonstrating high crystallinity and (c) selected area electron diffraction showing CdS cubic scattering profile of mesoporous network prepared from CdS NCs with a diameter of 4 nm (NCA-CdS-4).

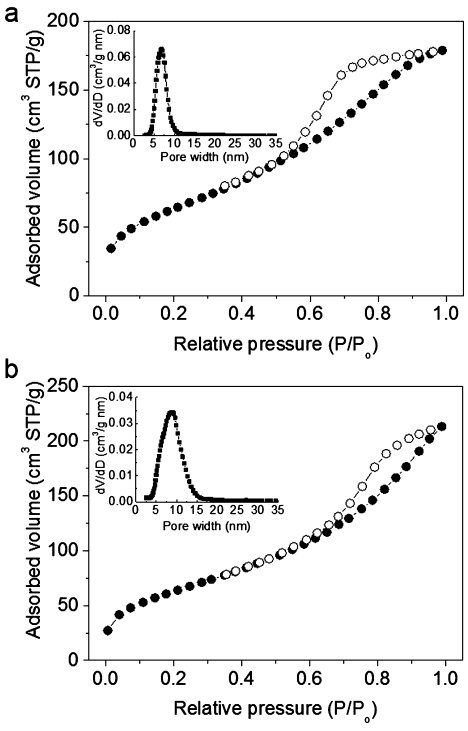

Figure 3. Nitrogen adsorption (solid symbols) and desorption (open symbols) isotherms at −196 °C for the two different mesoporous networks prepared from (a) 4 nm (NCA-CdS-4) and (b) 6.5 nm (NCA-CdS-6) size CdS NCs. Insets show the corresponding NLDFT pore size distributions calculated from the adsorption branch of isotherms.

234 $m^2\ g^{-1}$ and total pore volume is 0.28 $cm^3\ g^{-1}$. A similar surface area (230 $m^2\ g^{-1}$) and pore volume (0.30 $cm^3\ g^{-1}$) is obtained for mesoporous network of 6.5 nm CdS NCs (NCA-CdS-6). The pore size distributions assessed from the adsorption data using the nonlocal density functional theory (NLDFT) method was found to be quite narrow with a peak maximum of ~6.8 nm for NCA-CdS-4, consistent with the interparticle edge-to-edge distance observed from TEM (*ca.* 6 nm), and ~8.8 nm for NCA-CdS-6 (Figure 3, insets). On the basis of SAXS repeat distance and the NLDFT pore size, we derived an average pore wall thickness of about 7.5 and 10.8 nm for the mesoporous NCA-CdS-4 and NCA-CdS-6, respectively. Given the respective CdS particle size derived from SAXS data, these results indicate that an average of two NCs compose the thickness of the pore walls of materials. This is in line with TEM data. In comparison, we obtained an adsorption−desorption isotherm that is a combination of type-I and type-IV curves with an H_3 hysteresis loop for the RNA-CdS-4 sample, attributed to nanoporous solids with slit pores,[19] see Supporting Information Figure S6. The BET surface area of this material was measured to be 126 $m^2\ g^{-1}$, while NLDFT pore-size distribution analysis points to the formation of nanoparticle aggregates with ~2.6 nm-sized interstitial voids. Thus, the variations in surface area and pore width noted between the random aggregates and templated material are indicative to the different pore morphologies.

The mesoporous ensembles exhibit a well-defined electronic structure as interpreted by diffuse reflectance ultraviolet−visible/near-IR (UV−vis/NIR) spectroscopy (Figure 4a). The optical absorption spectra of mesoporous materials produced with different CdS building blocks show sharp absorption onsets associated with electronic transitions in the energy range from 2.50 eV (495 nm) for NCA-CdS-6 to 2.63 eV (471 nm) for NCA-CdS-4. This variation of energy gap with the diameter of the CdS NCs is associated with the size increase of the starting materials, supporting the notion that quantization electronic effects of the colloidal CdS NCs are persisted in assembled structures. Generally, the band gap energy of a fine semiconductor blue/hypsochromic shifts as the particle size decreases.[20,21] The resultant assemblies show a slightly narrow energy gap (~30−40 meV) compared with the energy gap of the respective CdS building blocks, manifesting a greater delocalization of the excitons (*i.e.*, a slight decrease in quantum confinement effect).

Emission properties of the 3-MPA-capped CdS NCs and resultant mesoporous assemblies were investigated using photoluminescense (PL) spectroscopy. As seen in Figure 4b, the mesoporous networks show an emission in the 1.6−2.7 eV range at room

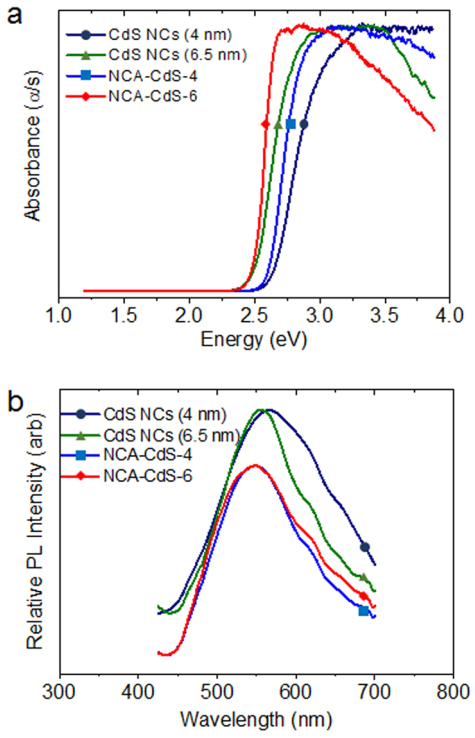

Figure 4. (a) Optical absorption and (b) room-temperature PL emission spectra of mesoporous ensembles produced with 4 and 6.5 nm-sized CdS NCs. The PL spectra are normalized to their maximum intensity. The corresponding spectra of the respective CdS nanobuilding blocks are also given.

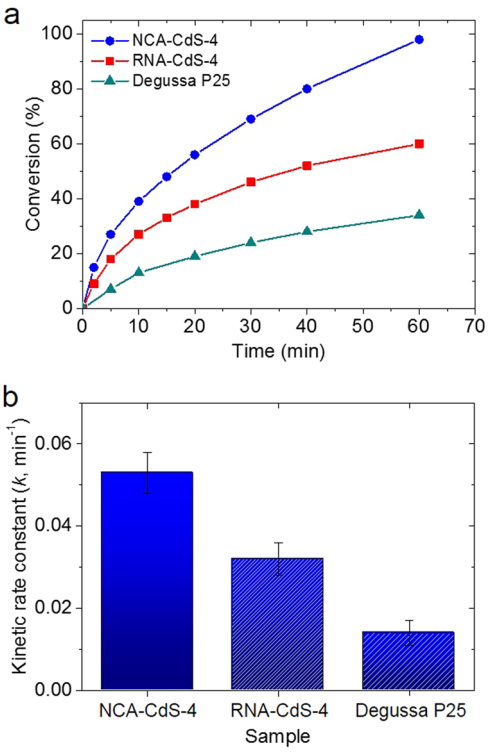

Figure 5. (a) Conversion of 1-phenylethanol to acetophenone as a function of irradiation time and (b) plot of kinetic rate constants of mesoporous NCA-CdS-4, random aggregates of 4 nm-sized CdS NCs (RNA-CdS-4) and TiO_2 Degussa (P25) nanoparticles. Reaction conditions: 0.2 mmol 1-phenylethanol, 0.25 mmol catalyst, O_2 bubbling (~1 mL/min), 3 mL benzene, 20 °C, visible-light irradiation (λ > 420 nm). The photooxidation over TiO_2 nanoparticles was performed in 3 mL of CH_3CN, under UV-light irradiation (λ > 320 nm).

temperature when excited with photons with high energy (380 nm). The peak maximum of the PL spectra (~2.3 eV) is located at wavelengths near the band-edge absorption of CdS, suggesting interband luminescence process (*i.e.*, between the quantized energy states of conduction and valence band), although contribution of surface and deep-level states to the emission process due to residual thiolate ligands cannot be excluded.[22] The photoemission energy of the mesoporous samples is very close to that of precursor NCs. This suggests that the assembly process does not significantly alter the PL response of the nanoscale CdS building blocks. The slight blue-shift in the PL spectra of assembled structures compared to the PL signal of individual CdS NCs (by ~30−50 meV) could be attributed to the low density of interband states due to the removal of thiolate ligands from nanocrystal surface. Also change in the effective quantum confinement resulting from some etching of the nanoparticles surface prior to assembly process is a possible explanation.[14]

More importantly, the present method is applicable to the synthesis of various mesoporous assemblies from metal chalcogenide NCs, including II−VI semiconductor nanoparticles such as ZnS. To test this expectation, we prepared porous ZnS-based assembled structure (NCA-ZnS-5) by using colloidal ZnS NCs with 5 nm size as starting materials. As follows from SAXS, TEM and N_2 physisorption experiments, the NCA-ZnS-5 sample possesses 3D mesoporous network of connected ZnS nanoparticles and shows BET surface area of 334 $m^2\ g^{-1}$, pore volume of 0.33 $cm^3\ g^{-1}$ and narrow pore size distribution at ~5.8 nm (Supporting Information Figures S7−S9). Just as in the CdS NC assemblies, the optical absorption properties in NCA-ZnS-5 are an intrinsic characteristic of the assembled network and depend on its ZnS NC constituents (see Supporting Information Figure S10).

Because of the large internal surface area, regular mesoscale pores and visible-light response, the present mesoporous NC-based assemblies are anticipated to sustain photocatalytic reactions. We evaluated the photocatalytic activity of NCA-CdS-4 mesoporous using visible light (wavelength (λ) > 420 nm) irradiated oxidation of 1-phenylethanol as a probe reaction. For comparison, we also evaluated the photooxidation of 1-phenylethanol to acetophenone over random aggregates of CdS NCs (RNA-CdS-4) as well as commercial TiO_2 Degussa (P25) catalyst (20−30 nm particle size, *ca.* 50 $m^2\ g^{-1}$), which is a well-known photoactive material (*i.e.*, Degussa P25 was selected as a benchmark catalyst). The evolution of photooxidation reaction presented in Figure 5a shows that NCA-CdS-4 exhibits

high reactivity toward 1-phenylethanol oxidation with a respective conversion factor of ~98% in 1 h. Indeed, the visible-light photocatalytic activity of NCA-CdS-4 greatly exceeds that of the random CdS NC aggregates (~60%) and Degussa P25 nanoparticles (~34%); notwithstanding that photoreaction of TiO_2 nanoparticles was examined under UV light ($\lambda > 320$ nm). Analysis of the catalytic data using the pseudo-first-order reaction model reveals that the reaction proceeds at a faster rate over mesoporous NCA-CdS-4 (kinetic constant (k) = 0.053 min^{-1}) than the random aggregates RNA-CdS-4 (k = 0.034 min^{-1}) and Degussa P25 nanoparticles (k = 0.014 min^{-1}) (see Figure 5b and Supporting Information Figure S11). Assuming that the oxygen concentration remains constant during the reaction, the oxidation of alcohol can be considered a pseudo-first order process, in which the reaction rate is proportional to the concentration of substrate. All these results consistently show that, despite the organic molecules remaining in pores (*ca.* 7−8 weight%), the pore surface of NCA-CdS-4 is photocatalytically active and accessible to the target molecules, contributing to the high catalytic activity. To our knowledge, the activity of NCA-CdS-4 compares also highest to the previous reported activities for high-performance O_2−CdS−1-phenylethanol catalytic systems, including porous aggregates of sheet-like CdS,[23] mesoporous $SiW_{12}O_{40}^{4-}/Ag_2S$/CdS heterostructures[24] and CdS/graphene nanocomposites[25] We suggest that the increase in photocatalytic performance observed in NCA-CdS-4 is related to the small grain size of CdS NCs, which minimize the distance that photogenerated electrons and holes need to reach the solid/liquid interface and the 3D open pore structure, which facilitates fast molecular transport and possibly efficient harvesting of light *via* multiple scattering within the assembled nanoparticles.[26] The NC-linked mesoporous networks we construct by this surfactant-templating process are quite stable under the present conditions. Catalyst regeneration experiments showed that high activity and selectivity are still retained after two consequent runs, giving quantitatively yield of acetophenone (>98%) in 1 h (Supporting Information Figure S12).

CONCLUSIONS

In summary, three-dimensional mesoporous networks of metal chalcogenide NCs can be prepared through a surfactant-assisted oxidative self-polymerization method, which involves controlled destabilization of colloidal metal sulfide nanoparticles in the presence of nonionic surfactants. Remarkably, this new assembly process has allowed us to construct ordered mesoporous architectures with different composition (*e.g.*, CdS and ZnS) and particle size (from 4 to 6.5 nm) of the chalcogenide nanobuilding blocks. Owing to the three-dimensional open pore structure, the NC ensembles of CdS showed high activity and stability in visible-light-driven oxidation of 1-phenylethanol into acetophenone. The proposed synthetic approach of linking metal chalcogenide nanoparticles together to construct ordered mesostructures opens up great opportunities for designing and fabricating new multifunctional materials. Such porous materials hold promise for potential technological applications in catalysis, energy storage and conversion, separation and chemical detection.

MATERIALS AND METHODS

Synthesis of CdS and ZnS NCs. CdS and ZnS NCs were prepared according to a modified literature procedure,[27,28] using cadmium chloride ($CdCl_2$) or zinc chloride ($ZnCl_2$) and sodium sulfide ($Na_2S \cdot 9H_2O$) as reagents and 3-mercaptopropionic acid (3-MPA) as capping agent. The chalcogenide NCs were isolated by precipitation with the addition of 2-propanol and dried at 60 °C for 18 h. For NCs with 4 nm diameter, a Cd:3-MPA:S composition of 1:2:1 (5.5 mmol $CdCl_2$, 11 mmol 3-MPA and 5.5 mmol $Na_2S \cdot 9H_2O$) was used, while with the use of a Cd:3-MPA:S molar composition of 1:1:1, CdS NCs with 6.5 nm in diameter were obtained. The 3-MPA-capped CdS NCs were redispersed in water to form stable colloidal dispersion with concentration of 100 mg mL^{-1}. For a Zn:3-MPA:S composition of 1:2:1, NCs of 5 nm in diameter were obtained. Highly concentrated (67 mg mL^{-1}) ZnS NC solutions were obtained by dispersing the 3-MPA-capped NCs in water.

Synthesis of Mesoporous CdS (and ZnS) NCAs. In a typical preparation of mesoporous CdS (and ZnS) NC assemblies, 250 mg of block copolymer Brij-58 ($HO(CH_2CH_2O)_{20}C_{16}H_{33}$, M_n ~ 1124) was dissolved in 2.5 mL of water inside a 50 mL glass beaker. To this solution, 3-MPA-capped CdS (or ZnS) NCs dispersed in 2.5 mL water (~1.7 mmol) was added and the resultant homogeneous dispersion was left stirring for an additional 1 h at room temperature. Then, 2 mL of 1 wt % H_2O_2 in water was added dropwised and the mixture was kept under stirring until gelation was observed (~1 h). The resultant mixture was placed in an oven for 3 days at 40 °C to evaporate the solvent under static conditions. Template removal was achieved by soaking the gel product once in 20 mL of ethanol for 2 h and three times in 20 mL of water for 15 min. The resultant mesoporous samples were filtrated under vacuum, washed several times with water and ethanol, and dried at 60 °C for 12 h.

Characterization. Thermogravimetric analysis (TGA) was performed using a Pelkin-Elmer Diamond system. Thermal analysis was conducted from 40 to 600 °C in a nitrogen flow of 100 mL min^{-1} with a heating rate of 5 °C min^{-1}. Small-angle X-ray scattering (SAXS) measurements were performed on a Rigaku S-MAX 300 high-brilliance system using Cu Kα radiation (80 kV and 40 mA). The sample-to-detector distance and center of the beam were precisely measured using a Ag-behenate standard (d_{001} = 58.38 Å). The two-dimensional diffraction images were integrated into a one-dimensional diffraction pattern, as a function of q, with the Fit2D program.[29] Scattering data were corrected for dark current and empty tube scattering. The average size of nanoparticles was determined from the scattering data, using the Guinier equation: $I(q) \propto \exp(-q^2R_g^2/3)$, where I is the scattering intensity and R_g is the radius of gyration, which is related to the diameter of spherical particles by the equation $D = 2R_g(5/3)^{1/2}$.[30] X-ray diffraction (XRD) patterns were collected on a PANanalytical Xpert Pro MPD X-ray diffractometer using Cu Kα radiation (45 kV and 40 mA) in Bragg−Brentano geometry. Transmission electron microscopy (TEM) images were taken with a JEOL JEM-2100 electron microscope

(LaB_6 filament) operating at an accelerated voltage of 200 kV. Samples were prepared by dispersing fine powders in ethanol using sonication, followed by depositing a drop of solution onto a holey carbon-coated Cu grid. Nitrogen adsorption–desorption isotherms were measured at −196 °C on a Quantachrome NOVA 3200*e* sorption analyzer. Prior to the measurement, all samples were outgassed at 80 °C under vacuum ($<10^{-5}$ Torr) for 12 h. The specific surface areas were calculated using the Brumauer-Emmett-Teller (BET) method[31] on the adsorption data in the relative pressure range of 0.05–0.26. The total pore volumes were estimated from the adsorbed amount at the relative pressure of $P/P_0 = 0.98$ and the pore size distributions were obtained from the adsorption branch of the isotherms, using the nonlocal density function theory (NLDFT) method.[32] Elemental compositions were obtained using a JEOL JSM-6390LV scanning electron microscope (SEM) operated at 20 kV. Data acquisition was performed using a 100 s accumulation time. Diffuse reflectance UV–vis/near-IR spectra were obtained on a PerkinElmer Lambda 950 optical spectrophotometer in the wavelength range 200–2500 nm. $BaSO_4$ powder was used as a 100% reflectance standard and base material on which the powder sample was coated. Diffuse reflectance data were converted to absorption using the Kubelka–Munk function $\alpha/S = (1-R)^2/(2R)$, where R is the measured reflectance, and α and S are the absorption and scattering coefficients, respectively. The band gaps of the samples were estimated from the onset of absorption data converted from reflectance.[33]

Photocatalytic Reactions. The photocatalytic reactions were carried out as follows: 0.2 mmol of substrate and 0.25 mmol of catalyst were added in 3 mL of benzene (or CH_3CN for Degussa P25) inside a 5 mL Pyrex glass reactor. Before switching on the lamp, the suspension was stirred for 30 min in the dark to homogeneously disperse the catalyst in the solution. Then the reaction was initiated by irradiation with a Variac Cermax 300 W Xe lamp, using a UV cutoff filter ($\lambda > 420$ nm). During irradiation, the reaction mixture was cooled with water bath (20 ± 2 °C) and bubbled with oxygen at a flow rate of ~1 mL min^{-1}. The products analysis was performed using a Shimadzu GC–MS QP2010 Ultra system equipped with a 60m Mega-5 MS capillary column. For recycling experiments, the photocatalyst was recovered by centrifugation, dried under vacuum at 60 °C, and used for the next catalytic run.

Conflict of Interest: The authors declare no competing financial interest.

Supporting Information Available: Thermogravimetric analysis; SAXS patterns of random aggregates of CdS NCs; Guinier plots for starting materials; N_2 sorption data for random aggregates of 4-nm-size CdS NCs; SAXS, TEM analysis, N_2 physisorption and optical absorption data for mesoporous ensembles of 5-nm ZnS NCs; catalytic results for photooxidation of 1-phenylethanol into acetophenone. This material is available free of charge *via* the Internet at http://pubs.acs.org.

Acknowledgment. We gratefully acknowledge financial support from the European Union and the Greek Ministry of Education (NSRF) under the ERC Grant Schemes (ERC-09, MESOPOROUS-NPs).

REFERENCES AND NOTES

1. Gaponik, N.; Wolf, A.; Marx, R.; Lesnyak, V.; Schilling, K.; Eychmüller, A. Three-Dimensional Self-Assembly of Thiol-Capped CdTe Nanocrystals: Gels and Aerogels as Building Blocks for Nanotechnology. *Adv. Mater.* **2008**, *20*, 4257–4262.
2. Watanabe, K.; Menzel, D.; Nilius, N.; Freund, H.-J. Photochemistry on Metal Nanoparticles. *Chem. Rev.* **2006**, *106*, 4301–4320.
3. Milliron, D. J.; Buonsanti, R.; Llordes, A.; Helms, B. A. Constructing Functional Mesostructured Materials from Colloidal Nanocrystal Building Blocks. *Acc. Chem. Res.* **2014**, *47*, 236–246.
4. Lua, Z.; Yin, Y. Colloidal Nanoparticle Clusters: Functional Materials by Design. *Chem. Soc. Rev.* **2012**, *41*, 6874–6887.
5. Nie, Z.; Petukhova, A.; Kumacheva, E. Properties and Emerging Applications of Self-Assembled Structures Made from Inorganic Nanoparticles. *Nat. Nanotechnol.* **2010**, *5*, 15–25.
6. Warren, S. C.; Messina, L. C.; Slaughter, L. S.; Kamperman, M.; Zhou, Q.; Gruner, S. M.; DiSalvo, F. J.; Wiesner, U. Ordered Mesoporous Materials from Metal Nanoparticle–Block Copolymer Self-Assembly. *Science* **2008**, *320*, 1748–1752.
7. Rauda, I. E.; et al. General Method for the Synthesis of Hierarchical Nanocrystal-Based Mesoporous Materials. *ACS Nano* **2012**, *6*, 6386–6399.
8. Buonsanti, R.; Pick, T. E.; Krins, N.; Richardson, T. J.; Helms, B. A.; Milliron, D. J. Assembly of Ligand-Stripped Nanocrystals into Precisely Controlled Mesoporous Architectures. *Nano Lett.* **2012**, *12*, 3872–3877.
9. Mohanan, J. L.; Arachchige, I. U.; Brock, S. L. Porous Semiconductor Chalcogenide Aerogels. *Science* **2005**, *307*, 397–400.
10. Rauda, I. E.; Saldarriaga-Lopez, L. C.; Helms, B. A.; Schelhas, L. T.; Membreno, D.; Milliron, D. J.; Tolbert, S. H. Nanoporous Semiconductors Synthesized Through Polymer Templating of Ligand-Stripped CdSe Nanocrystals. *Adv. Mater.* **2013**, *25*, 1315–1322.
11. Qi, L.; Cölfen, H.; Antonietti, M. Synthesis and Characterization of CdS Nanoparticles Stabilized by Double-Hydrophilic Block Copolymers. *Nano Lett.* **2001**, *1*, 61–65.
12. Zhang, H.; Hyun, B.-R.; Wise, F. W.; Robinson, R. D. A. Generic Method for Rational Scalable Synthesis of Monodisperse Metal Sulfide Nanocrystals. *Nano Lett.* **2012**, *12*, 5856–5860.
13. Arachchige, I. U.; Brock, S. L. Sol–Gel Assembly of CdSe Nanoparticles to Form Porous Aerogel Networks. *J. Am. Chem. Soc.* **2006**, *128*, 7964–7971.
14. Pala, I. R.; Arachchige, I. U.; Georgiev, D. G.; Brock, S. L. Reversible Gelation of II–VI Nanocrystals: The Nature of Interparticle Bonding and the Origin of Nanocrystal Photochemical Instability. *Angew. Chem., Int. Ed.* **2010**, *49*, 3661–3665.
15. Pileni, M. P. Supracrystals of Inorganic Nanocrystals: An Open Challenge for New Physical Properties. *Acc. Chem. Res.* **2008**, *41*, 1799–1809.
16. Lu, Z.; Yin, Y. Colloidal Nanoparticle Clusters: Functional Materials by Design. *Chem. Soc. Rev.* **2012**, *41*, 6874–6887.
17. Scherrer, P. Bestimmung der Größe und der inneren Struktur von Kolloidteilchen mittels Röntgenstrahlen. *Göttinger Nachr. Math.-Phys.* **1918**, *2*, 98–100.
18. Thommes, M. In *Nanoporous Materials: Science and Engineering*; Lu, G. Q.; Zhao, X. S., Eds.; Imperial College Press: London, U.K., 2004, Ch. 11.
19. Rouquerol, F.; Rouquerol, J.; Sing, K. S. W. In *Adsorption by Powders and Porous Solids. Principles, Methodology and Applications*; Academic Press: London, U.K., 1999.
20. Alivisatos, A. P. Semiconductor Clusters, Nanocrystals, and Quantum Dots. *Science* **1996**, *271*, 933–937.
21. Brus, L. E. Electron–Electron and Electron-Hole Interactions in Small Semiconductor Crystallites: The Size Dependence of the Lowest Excited Electronic State. *J. Chem. Phys.* **1984**, *80*, 4403–4409.
22. Okamoto, S.; Kanemitsu, Y. Photoluminescence Properties of Surface-Oxidized Ge Nanocrystals: Surface Localization of Excitons. *Phys. Rev. B* **1996**, *54*, 16421–16424.
23. Zhang, Y.; Zhang, N.; Tang, Z.-R.; Xu, Y.-J. Transforming CdS into an Efficient Visible Light Photocatalyst for Selective Oxidation of Saturated Primary C–H Bonds under Ambient Conditions. *Chem. Sci.* **2012**, *3*, 2812–2822.
24. Kornarakis, I.; Lykakis, I. N.; Vordos, N.; Armatas, G. S. Efficient Visible-Light Photocatalytic Activity by Band Alignment in Mesoporous Ternary Polyoxometalate–Ag_2S–CdS Semiconductors. *Nanoscale* **2014**, *6*, 8694–8703.
25. Zhang, N.; Zhang, Y.; Pan, X.; Fu, X.; Liu, S.; Xu, Y.-J. Assembly of CdS Nanoparticles on the Two-Dimensional Graphene Scaffold as Visible-Light-Driven Photocatalyst for Selective Organic Transformation under Ambient Conditions. *J. Phys. Chem. C* **2011**, *115*, 23501–23511.

26. Yu, J. C.; Wang, X. C.; Fu, X. Z. Pore-Wall Chemistry and Photocatalytic Activity of Mesoporous Titania Molecular Sieve Films. *Chem. Mater.* **2004**, *16*, 1523–1530.
27. Li, H.; Shih, W. Y.; Shin, W. H. Synthesis and Characterization of Aqueous Carboxyl-Capped CdS Quantum Dots for Bioapplications. *Ind. Eng. Chem.* **2007**, *46*, 2013–2019.
28. Sobhana, S. S. L.; Devi, M. V.; Sastry, T. P.; Mandal, A. B. CdS Quantum Dots for Measurement of the Size-Dependent Optical Properties of Thiol Capping. *J. Nanopart. Res.* **2011**, *13*, 1747–1757.
29. Hammersley, F. A. P. In *ESRF98HA01T: FIT2D V9.129 Reference Manual v3.1*, ESRF—Internal Report, France, **1998**.
30. Schmidt, P. W. in *Modern Aspects of Small-Angle Scattering*; Kluwer Academic Publishers, Dordrechr, The Netherlands, 1995.
31. Brunauer, S.; Deming, L. S.; Deming, W. S.; Teller, E. On a Theory of the van der Waals Adsorption of Gases. *J. Am. Chem. Soc.* **1940**, *62*, 1723–1732.
32. Ravikovitch, P. I.; Wei, D.; Chueh, W. T.; Haller, G. L.; Neimark, A. V. Evaluation of Pore Structure Parameters of MCM-41 Catalyst Supports and Catalysts by Means of Nitrogen and Argon Adsorption. *J. Phys. Chem. B* **1997**, *101*, 3671–3679.
33. Kubelka, P. New Contributions to the Optics of Intensely Light-Scattering Materials. Part I. *J. Opt. Soc. Am.* **1948**, *38*, 448–448.